Solid-state phase transformation in a lithium disilicate-based glass-ceramic

Serge Barone, Alexandre Freulon, Benoît Malard, Moukrane Dehmas

Solid-state phase transformation in a lithium disilicate-based glass-ceramic

Serge Barone[a], Alexandre Freulon[b], Benoit Malard[b], Moukrane Dehmas[a,b,*]

[a] Institut Jean Lamour (IJL), UMR 7198, CNRS-Université de Lorraine, Nancy, France
[b] CIRIMAT, Université de Toulouse, CNRS, Toulouse, France

Keywords:
Microstructure
Lithium disilicate
Glass ceramic
Quantitative analysis

The solid-state phase transformation in a lithium disilicate-based glass-ceramic (IPS e.max® CAD) was revisited on the basis of quantitative data. IPS e.max® CAD is widely used as material for the dental restoration in the dental industry. In-situ X-ray diffraction and differential scanning calorimetry accompanied by scanning electron microscopy observations were applied to understand phase transformation during heat treatment in a dental ceramic. In-situ X-ray diffraction evidences the concomitant formation of cristobalite and lithium orthophosphate at 770 °C. Then, the formation of lithium disilicate occurred at the expense of a complete dissolution of cristobalite and lithium metasilicate. No phase transformation occurred during cooling. The quantitative results of microstructural features (amount of each phase, morphology, and number density of lithium disilicate and lithium metasilicate) indicate that lithium disilicate is probably formed by diffusional process at the lithium metasilicate/cristobalite interface, which acts as favorable nucleation sites. The energy barrier is probably too high for lithium disilicate nucleation in the amorphous matrix. The quantitative results will provide the background for further modeling of phase transformation kinetics, which may have potential industrial benefits.

1. Introduction

Over the last decade, the development of new dental crowns has undergone rapid expansion with the huge interest in cosmetic dentistry. The actors in this sector aim to produce ceramic crowns that are more transparent and sustainable (e.g. preventing the appearance of a grey border at the base of the tooth) over time. From ceramic crowns, the development of Lithium Disilicate Glass Ceramic (LD GC) has been a milestone at that respect [1,2]. Among the LD GCs, IPS e.max® CAD bloc is widely used as material for dental crowns and three unit bridge for anterior teeth. At the end of solidification, the microstructure of the IPS e.max® CAD bloc is partially crystallized and is fine with many li thium metasilicate precipitates of uniform size homogeneously dis persed in an amorphous matrix. Such a microstructure strongly affects the mechanical properties, and hence their potential engineering ap plications. Therefore, a second heat treatment needs to be performed in order to get a fully crystallized state and thus obtain the appropriate mechanical properties. Extensive research [3 6] was carried out on the study of thermal decomposition of the lithium metasilicate (Li_2Si0_3, LS) but the detailed pathways of phase transformation were not clarified. According to the previous studies, it is commonly admitted that the sequence of the phase transformation in this system during heat treat ment is: $SiO_2 + Li_2SiO_3 \rightarrow Li_2Si_2O_5$ [5]. The mechanical properties after heat treatment are due to the interlocked microstructure and the morphology of the precipitates [7] as well as the thermal path and the nominal chemical composition [8 12]. As an example, a good bending strength is achieved by lithium disilicate ($Li_2Si_2O_5$, LS2) crystals in corporated in the amorphous matrix. Thus, a flexural strength of the order of 400 MPa higher than that of dentin is obtained [13 15].

The nucleation of lithium disilicate takes place around 800 °C in the presence of a P_20_5 catalyst. Volume and surface nucleation mechanisms have been proposed with a predominance that depends on the nominal chemical composition and the nucleating agents [16]. The P_2O_5 oxide would promote the nucleation rate of LS2 precipitates that act as the heterogeneous nucleation sites via the formation of lithium orthopho sphate precipitates (Li_3PO_4, LP) in Li rich regions at low temperature [17,18]. The higher the amount of P_2O_5 oxide, the smaller the size of the LS2 precipitates to become spherical. The optimum concentration for maintaining good mechanical properties is between 1.0 mol% and 2.5 mol% P_2O_5 [18]. Other studies have shown that during the phase transformation, β cristobalite and lithium disilicate grow by epitaxy on lithium orthophosphates [4]. The growth kinetics of LS2 could be ac celerated when the maximum formation of Li_2SiO_3 has ended [19] [20] and the β cristobalite could contribute to the phase transformation [19].

Despite a large number of investigations, most of the proposed

* Corresponding author at: CIRIMAT, Université de Toulouse, CNRS, INP- ENSIACET 4 allée Emile Monso, BP44362, 31030 Toulouse, Cedex 4, France.
E-mail address: moukrane.dehmas@ensiacet.fr (M. Dehmas).

https://doi.org/10.1016/j.jnoncrysol.2019.03.006

mechanisms are based on assumptions because the fineness of the microstructure makes it difficult to obtain quantitative results such as the chemical composition, the size or the number density of precipitates. Consequently, the quantitative aspects of the microstructure evolution are poorly documented. Huang et al. quantified the evolution kinetics of the different phases involved during heat treatment by in situ synchrotron X ray diffraction [3]. However, they did not discuss of the interdependence of changes in Li rich phases and β cristobalite formation. These considerations prompted the present study that is focused on this interdependence. Following an initial illustration of the microstructural changes associated with heat treatment, when applied under conditions of dental laboratories, a quantitative analysis is made of the simultaneous evolution of LS, LS2 and β cristobalite. Variations in the quantity, morphology, and number density of the phases are reported and discussed.

2. Material and methods

The investigated material is a multicomponent system with a wide composition range (in wt%) of 57 80 SiO_2, 11 19 Li_2O, 0 13 K_2O, 0.5 11 P_2O_5, 0 8 ZrO_2, 0 8 ZnO, 0 5 MgO, 0 5Al_2O_3 and 0 8 coloring oxides [21]. This multicomponent system is marketed by Ivoclar Vivadent company under the trade name of IPS e.max® CAD.

The phase identification at room temperature was performed on a D8 Advanced diffractometer (Bruker), using Cu radiation from a generator equipped with a curved monochromator. The acquisition time was 1 h under a voltage of 35 kV and an emission current of 20 mA for an angular (2θ) range of 15° 120° (step width of 0.016°).

In situ X Ray Diffraction (XRD) experiments were carried out with an X'Pert Pro diffractometer (PANalytical) equipped with a Cu anticathode and a high speed multichannel X'Celerator detector at very high count rates. The heating was provided by an Anton Paar HTK 1200 resistance heating chamber under primary vacuum. The calibration in temperature of the heating device was checked by measuring the thermal expansion of an external standard phase (silicon) and a known phase transition (quartz). The diffractograms were collected in an angular (2θ) range 10 45° and over a temperature range 25 500 °C at intervals of 50 °C, and 500 850 °C at intervals of 25 °C. The temperature ramp between two consecutive temperatures on heating and cooling was both 60 °C/min. The sample was kept at temperatures for 3 min before collecting the diffractogram during 15 min. The XRD line profile analysis was carried out by Rietveld Method [22,23] on the Fullprof 2 K software [24] developed by Carvajal et al. [25]. For each pattern, the following parameters were refined: scale factors, peak breadth, lattice parameters and Debye Waller factor. The resulting Rietveld refinement gives the mass fraction and the mean lattice parameters of the phases.

In order to precise the temperature range of phase transformation, Differential Scanning Calorimetry (DSC) curves were obtained with a high temperature multi HTC Setaram scanning calorimeter. A sample of 4 mm in diameter and 6 mm in length was placed in alumina pan. The pan was then placed in the DSC head together with a reference pan and protected by a high purity nitrogen atmosphere with a gas flow speed of 60 ml.min^{-1}. External standard In, Zn, Al, Cu, Ni samples were heated at the temperature higher than melting temperature for the calibration of heat flow and temperature. A heating rate of 50 °C/h from ambient to 850 °C was adopted in order to obtain a right balance in temperature between the two pans, however, sufficient so that the phase transformation appears clearly. Three samples were analyzed to ensure the repeatability.

To obtain further clarification on the phase transformation occurred during heat treatment, the microstructure of the bulk sample at the as received state, as well as after heat treatment was imaged with the aid of a field emission scanning microscope Philips XL30 SFEG under a 10 kV acceleration voltage. Quantitative analysis of the micrographs was made using Aphelion® Software on at least 50 images per sample to determine representative mean values of the characteristic parameters (i.e. surface fraction, particle size and number density). Sample preparation consisted of mechanical grinding followed by diamond and final OPS (oxide polishing suspension) polishing, and observed without prior etching in backscattered electron mode.

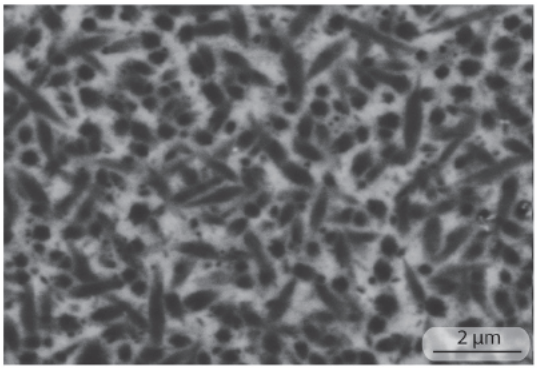

Fig. 1. BSE micrograph of the typical microstructure of the IPS e.max® CAD in the as-received state (the stick-shaped precipitates is in dark grey and the matrix is white). The sample was observed without prior etching so as not to significantly alter the shape of precipitates.

The heat treatment was chosen on the basis of what most dental laboratories commonly applied. The sample was heated in the porcelain furnace (Programat CS, Ivoclar Vivadent). The applied heat treatment was: heating to 850 °C with a rate of 100 °C/min; isothermal holding for 3 min; furnace cooling to room temperature in the primary vacuum.

3. Results

3.1. As received state

Fig. 1 shows a typical microstructure of the as received state. The microstructure consists of the very small stick shaped precipitates surrounded by a matrix. The stick shaped precipitates are not faceted and are randomly orientated suggesting that there is no specific orientation relationship with the matrix. A precise quantitative chemical analysis of the precipitates was not attempted due to their extremely small size.

In contrast, the X ray diffractogram (Fig. 2) displays the presence of a very high background and a broad hump. The 2θ angular position of the broad hump is around 23°. This feature is indicative of the amorphous structure. According to the phase diagram for the $Li0_2$ $Si0_2$ system, $Si0_2$ is expected. In addition, several sharp diffraction peaks can be observed, which are indexed as an orthorhombic structure with $Cmc2_1$ space group from the Pearson's Crystal Data database. The mean lattice parameters were calculated to be a = 9.408 Å, b = 5.413 Å and c = 4.665 Å, which are in good agreement with the reported values of LS. Consequently, the stick shaped precipitates visible by SEM correspond to LS and the matrix to the amorphous structure.

The X ray diffractogram was also analyzed with Fullprof software [24] using the Rietveld method [22,23] in order to determine the mass fraction of amorphous matrix and LS. The volume fraction was then calculated by considering the density of each phase. The structural model used for the Rietveld refinement is based on the following structural data: an orthorhombic structure with $Cmc2_1$ space group for the LS phase and a cubic structure of SiO_2 with $P2_13$ space group for the amorphous phase. It is noteworthy that amorphous $Si0_2$ phase may contain other solute elements that can affect the quantitative analysis. In the case of the amorphous phase, a micro crystallinity model that takes into account micro strain is considered. Therefore, the amorphous phase can be described as a nanocrystalline structure, leading to strong line broadening on the X ray diffractogram. This model, originally proposed by Le Bail [26], was successfully used to determine amorphous silica content in the case of ceramic materials [27]. The quality of the refinement was confirmed by a visual examination of the plotted

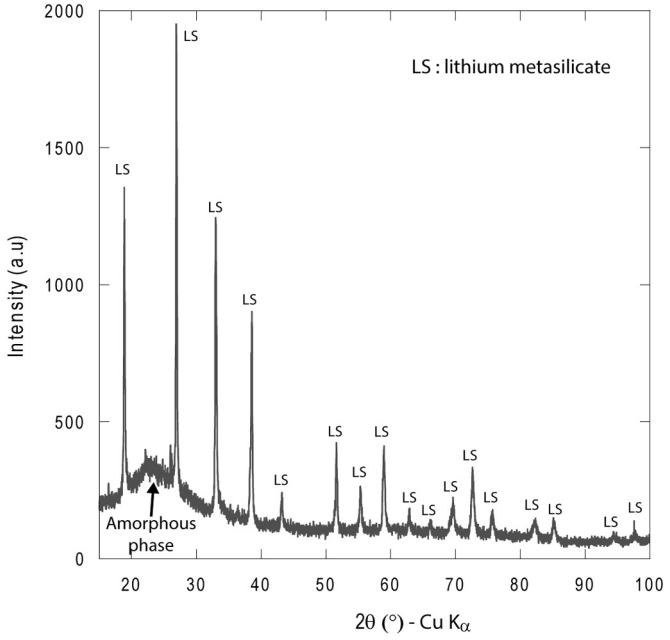

Fig. 2. X-Ray diffractogram at room temperature of the IPS e.max® CAD in the as-received state and the corresponding identified phases.

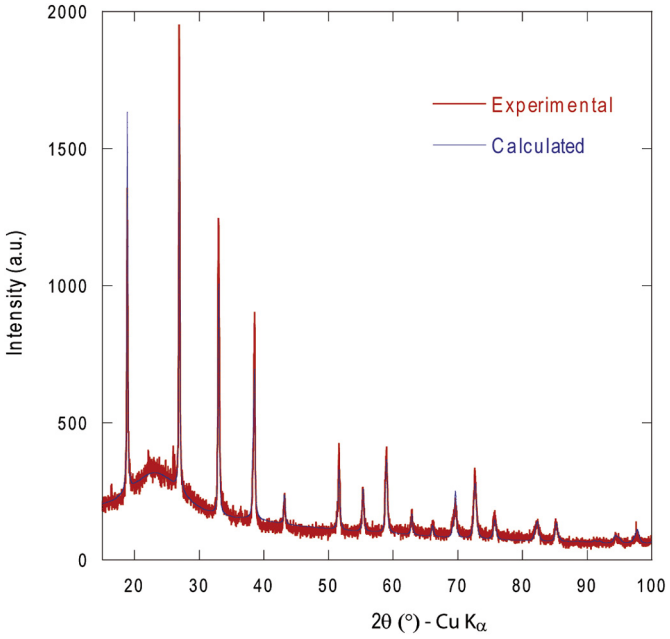

Fig. 3. Experimental and calculated (Rietveld refinement) XRD patterns for the IPS e.max® CAD in the as-received state at room temperature.

difference between the measured and calculated profiles as shown in Fig. 3 and by the reliability factors Rwp, which is lower than 10. The volume fraction of LS was found to be 40%.

The volume fraction of LS determined by Rietveld refinement was compared to that determined by image analysis in order to validate the hypothesis that the amorphous phase can be described as a nanocrystalline structure in the model. Thus, the volume fraction was found to be 42%, which implies that the data processing methods are self consistent and have acceptable precision. In addition, the average length and width of the LS precipitates were 0.8 µm and 0.25 µm, respectively. The number density was $1.5.10^{-6}$ particles/mm^2.

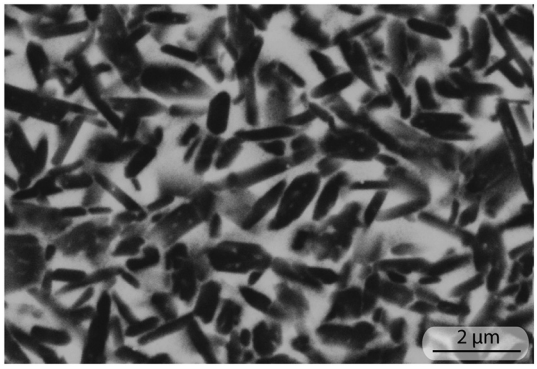

Fig. 4. BSE micrograph of the final microstructure of the IPS e.max® CAD aged at 820 °C for 3 min with a heating rate of 100 °C/min and furnace cooling to room temperature (the stick-shaped precipitates is in dark grey and the matrix is white). The sample was observed without prior etching so as not to significantly alter the shape of precipitates.

3.2. Characterization after heat treatment

The resulting microstructure after heat treatment is shown in Fig. 4. No significant difference was found in the spatial distribution of the precipitates and in the number density ($1.5.10^{-6}$ precipitates/mm^2). However, the average length (0.95 µm) and width (0.3 µm) of the stick shaped precipitates are higher as compared to the as received state and their shape appears to be much more faceted.

Fig. 5 displays the XRD pattern recorded after heat treatment. This pattern was consistently indexed on the basis of amorphous phase and orthorhombic, LS2 type structure (space group: C1c1) identified from the Pearson's Crystal Data database with the mean lattice parameters: a = 5.843 Å, b = 14.624 Å and c = 4.784 Å. Traces of Li_3PO_4 was also detected. The volume fraction of LS2 calculated by Rietveld refinement was found to be 60%, and is in agreement with the value obtained by image analysis. Based on this quantitative approach, it can be considered that a complete conversion of LS was achieved after heat treatment and that a substantial part of the amorphous phase (20%)

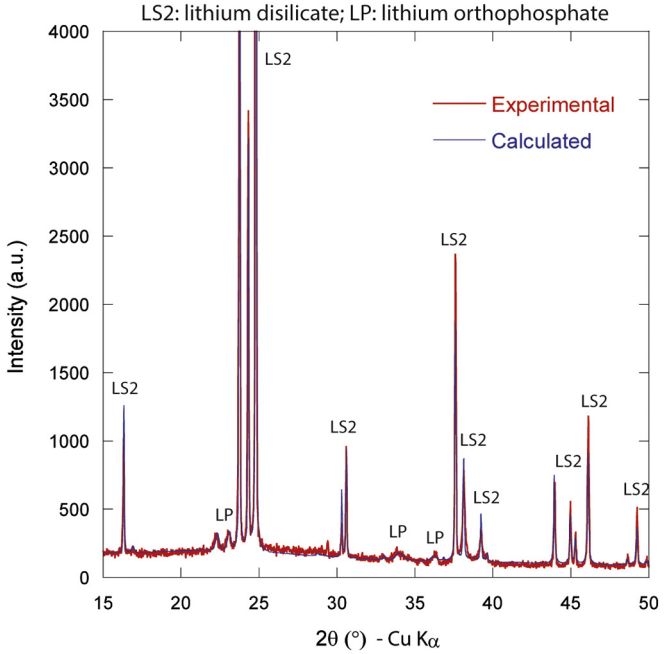

Fig. 5. Experimental and calculated (Rietveld refinement) XRD patterns for the IPS e.max® CAD aged at 820 °C for 3 min with a heating rate of 100 °C/min and furnace cooling to room temperature.

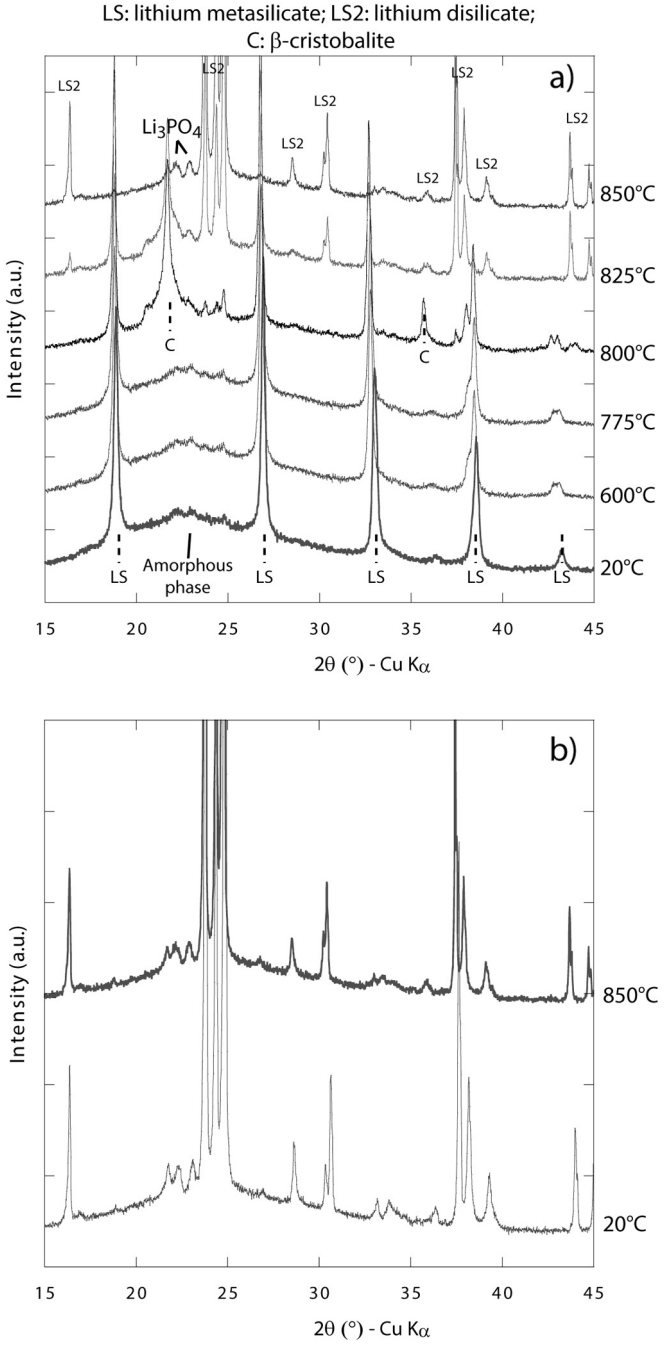

Fig. 6. In-situ X-ray diffractograms of the IPS e.max® CAD: a) heating at 60 °C/min interrupted by isothermal holding steps; b) 850 °C and at room temperature after a cooling rate of 60 °C/min.

was transformed into LS2.

3.3. In situ characterization of phase transformation

For a better understanding of the structural changes during heat treatment, further characterizations were developed. Fig. 6a displays the XRD pattern recorded on heating. From room temperature to 775 °C, only amorphous phase and Li_2SiO_3 phase are confirmed. In this temperature range, the peak positions of Li_2SiO_3 phase are shifted to lower angles or higher interplanar spacing, indicating thermal expansion of the phase. At 800 °C, the presence of the new phase is detected. This phase was indexed as β cristobalite (SiO_2) cubic structure with Fd3m space group and a mean lattice parameter of 7.137 Å [28]. The β cristobalite is considered as stable above 1470 °C [29] but can exist as metastable at lower temperature [30]. The Rietveld refinement of the XRD pattern with the three phases (amorphous phase, Li_2SiO_3 and β cristobalite) gives the following volume fractions: 40% amorphous phase, 20% β cristobalite and 40% Li_2SiO_3. The volume fraction of Li_2SiO_3 do not change as compared to the as received state. This means a partial crystallization of amorphous matrix.

At 825 °C, a new phase began to appear and the volume fractions of β cristobalite and Li_2SiO_3 decreased. This new phase can be assigned to the LS2 ($Li_2Si_2O_5$). The volume fraction of β cristobalite, LS and LS2 was found to be 7%, 23% and 28%, respectively. It is noteworthy that the volume fraction of amorphous phase remains constant (42 vol%). Based on this observation, we can conclude that the formation of LS2 at the expense of LS requires a partial crystallization of the amorphous matrix.

At 850 °C, it can be found a complete transformation of β cristobalite and Li_2SiO_3 into $Li_2Si_2O_5$. The volume fractions of $Li_2Si_2O_5$ and amorphous phase were found to be 60% and 40%, respectively. Traces of Li_3PO_4 were also detected with very low volume fraction when β cristobalite appeared. During cooling, no obvious change is observed, with the exception of the angular positions that are shifted due to the thermal contraction (Fig. 6b). Fig. 7 gives the DSC curve with exothermic reaction in the range of 770 °C and 830 °C whose area is proportional to the volume fraction. The temperature reaction domain is comparable to that identified by in situ XRD. Moreover, the observed shoulder suggests two distinct mechanisms that could correspond to those also identified by in situ XRD.

The mean lattice parameters of LS were also determined during heat treatment. The relative lattice parameter evolutions of LS on heating are displays in Fig. 8a. In the temperature range 20 °C and 775 °C, the mean lattice parameters follow linear expansion trend. The apparent Coefficient of Thermal Expansion (CTE) along the a and b directions of LS phase are in the same order of magnitude and are close to $20.10^{-6}K^{-1}$. The CTE along the c direction was found to be close to $13.10^{-6}K^{-1}$. Above 775 °C, as the transformation occurs, a deviation from linearity is observed, regardless of the lattice parameter. These deviations are probably caused by the formation of β cristobalite because no significant variation in solubility in the LS phase is expected

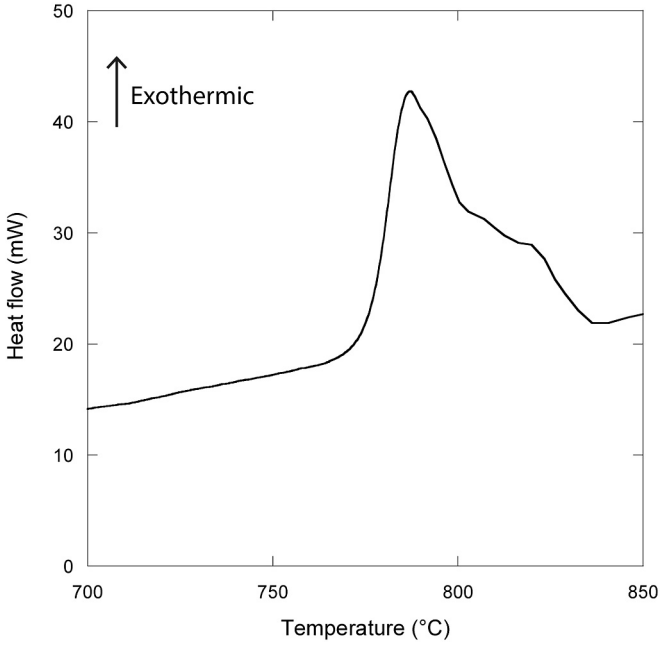

Fig. 7. DSC thermogram recorded at a heating rate of 50 °C/min from ambient to 850 °C of the IPS e.max® CAD. The figure displays an enlargement of the restricted temperature domain, to show the exothermic peak appearance.

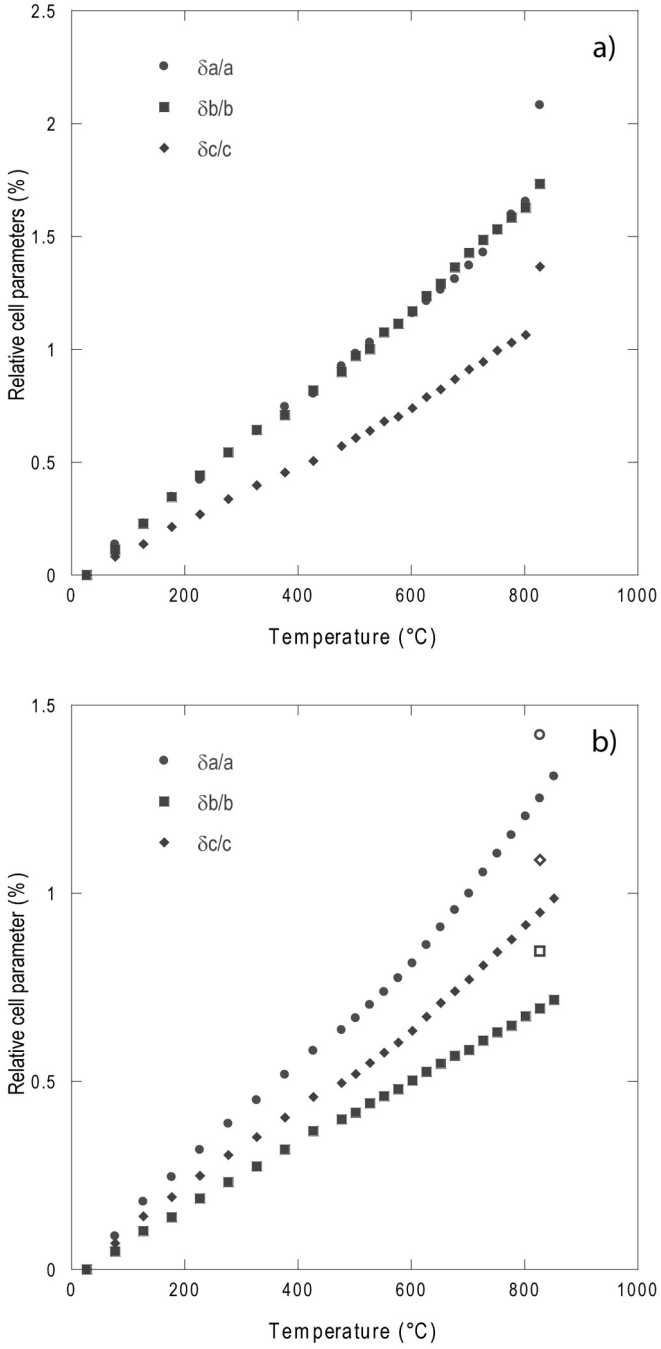

Fig. 8. Evolution of relative lattice parameters: a) LS during heating at 60 °C/min interrupted by isothermal holding steps; b) LS2 during cooling at 60 °C/min interrupted by isothermal holding steps. The open symbols are the measures of lattice parameters of LS2 relating to the end of the heating. The accuracy of the calculated mean lattice parameters is close to 1.10^{-3} Å.

with temperature according to the phase diagram of the $Li0_2$ $Si0_2$ system. The relative lattice parameters evolutions of LS2 at the end of the heating and during cooling are shown in Fig. 8b. The open symbols are the measures of lattice parameters of LS2 relating to the end of the heating. We can see that the mean lattice parameters are clearly different at equivalent temperature (825 °C), which implies a large contribution of the involved phases (β cristobalite and LS) on the internal stress state. During cooling, the mean lattice parameters progress linearly with a slope change at about 500 °C. The respective slopes for each lattice parameter notably change regardless of the considered temperature domain.

4. Discussion

The complementarity of techniques allowing microstructural observation (SEM) and the identification of phases (XRD) made it possible to highlight the microstructural changes during a heat treatment in a glass ceramic containing LS as crystalline phase. Thus, it has been possible to monitor on heating the transformation of LS (metastable phase) into LS2 (stable phase) in the temperature range between 775 °C and 850 °C. The temperature range is fairly similar to that determined by Lien el al. [20], which consider that the phase transformation kinetics is rapid. In our study, we showed that this phase transformation can be described by two stages that are quite distinct:

60% Residual glass + 40% LS → 40% Residual glass + 20% β cristobalite + 40% LS.

40% Residual glass + 20% β cristobalite + 40% LS → 40% Residual glass + 60% LS2.

At first stage, β cristobalite is nucleated at the LS/amorphous matrix interface because the number density of crystalline phase remains constant after heat treatment and then grow at the expense of the amorphous matrix. At the second stage, LS2 precipitates are nucleated at the LS/β cristobalite interface and then grow at the expense of the LS and β cristobalite.

The transformation requires the concomitant formation of a sufficient amount of β cristobalite and lithium orthophosphate. Many works report the same finding without providing any explanation of the mechanisms involved. Most authors assume that the lithium orthophosphate precipitates facilitate the formation of LS2 by acting as a heterogeneous nucleation site [31] while others suggest that the lithium orthophosphate precipitates are less likely to increase the nucleation rate of LS2 [4].

In our current study, quantitative image analysis showed that the number density of LS2 precipitate after heat treatment is similar to that of LS in the as received state. Only the average size increases after heat treatment with more faceted shapes compared to that in the as received state. The similar number density before and after heat treatment indicates that the nucleation of LS2 occurs mainly at pre existing interfaces. Thus, the nucleation of LS2 precipitates inside the amorphous matrix can be considered negligible. These results suggest also that the growth of LS2 is not governed by a coalescence regime, which means that the phase transformation takes place without long range diffusion, with mass transport on the distance scale of the LS precipitate in the amorphous matrix.

LS2 is nucleated at the LS/β cristobalite interface. This hypothesis is supported again by the number density of crystalline phase, which remains constant after heat treatment and by the shape of LS2 precipitates after heat treatment, which often exhibits a more faceted stick shape as compared to the as received state. In the case of a crystalline phase surrounded by an amorphous phase, the shape is often determined by minimizing the elastic strain energy and the interfacial energy is negligible. For a crystalline phase surrounded by a crystalline matrix (β cristobalite in our case), the growth is expected to take place in configurations that ensure a minimum of strain and interfacial energies. Consequently, the more faceted shape of LS2 precipitates can be explain by the prior nucleation of β cristobalite at the LS/amorphous matrix interface, before that of the LS2 precipitates. Lien et al. [20] also showed an evolution in the shape of crystalline phases as a function of temperature range (e.g. irregularly oblate like precipitates of LS2 above 780 °C). Moreover, the transformation of amorphous phase into β cristobalite at the LS/amorphous matrix interface is accompanied by a change of free energy, including strain energy in individual phase and interfacial energy LS/β cristobalite. This change probably reduces the nucleation barrier and enhances the solute diffusion.

Glass crystallization in the studied system is an extremely complex process because a large number of parameters can play a role in its temperature stabilization. It is commonly admitted that the crystallization rate of the amorphous phase can be thus controlled by adding

nucleating agents or by applying heat treatment and/or pressure [32].

One of the explanation would be that the glass crystallization might be due to a strong thermodynamic stability at high temperature of the β cristobalite. However, this hypothesis is rejected because it would lead to a complete crystallization of the amorphous phase. Two other explanations might be given by considering a local change in the state of internal stress and a local change in the chemical composition of the amorphous phase.

The changes in mean lattice parameters of lithium metasilicate have shown that this phase expands strongly on heating. This expansion can lead to a compressive state of the amorphous phase on heating and thus create a nanocrystalline periodicity [33]. However, the spatial dis tribution of the stick shaped precipitates (small spacing between the sticks) assumes that the distribution of strain field is relatively homo geneous and consequently that the crystallization rate is much greater than that measured experimentally by in situ XRD.

A local change in the chemical composition of the amorphous phase appears to be the most reasonable hypothesis. Indeed, it is very likely that the local equilibrium at the LS/amorphous matrix interface change as a function of temperature. In this case, a change in this local equi librium would be accompanied by the solute diffusion such that the chemical composition in the phases would continually and gradually change towards thermodynamic equilibrium. To prove the presence of the concentration gradient in the amorphous matrix at the LS/amor phous matrix interface, it is necessary to access the local chemical composition of each phase and their kinetics evolution. The identifi cation of concentration gradient will be difficult to demonstrate due to the rapid diffusivity of light elements such as lithium.

5. Conclusion

The transformation of lithium metasilicate into lithium disilicate has been studied by in situ X ray diffraction and microstructural ob servations coupled with quantification tools developed to evaluate the evolution of the microstructural parameters during heat treatment.

This study has confirmed previous observations of the simultaneous presence of β cristobalite and lithium orthophosphate during the transformation of lithium metasilicate into lithium disilicate on heating. In addition, based on quantitative analyzes, a probable me chanism is proposed for the phase transformation. Thus, the pre cipitation of β cristobalite probably takes place by diffusional nuclea tion and growth at the LS/amorphous matrix interface and its presence probably leads to a reduction in the nucleation barrier of lithium dis ilicate. In addition, the driving force is not enough for the nucleation of LS2 in the amorphous matrix. The quantitative analysis will provide the background for further modeling of phase transformation kinetics, which may have potential industrial benefits.

Acknowledgements

The authors would like to thank Ghouti Medjahdi for the XRD ex periments and MEM competence center for the SEM observations.

References

[1] R.W. Wassell, A.W.G. Walls, J.G. Steele, Crowns and extra-coronal restorations: materials selection, Br. Dent. J. 192 (2002) 199–211, https://doi.org/10.1038/sj.bdj.4801334.

[2] P. Boitelle, B. Mawussi, L. Tapie, O. Fromentin, A systematic review of CAD/CAM fit restoration evaluations, J. Oral Rehabil. 41 (2014) 853–874, https://doi.org/10.1111/joor.12205.

[3] S. Huang, P. Cao, Y. Li, Z. Huang, W. Gao, Nucleation and crystallization kinetics of a multicomponent lithium disilicate glass by in situ and real-time synchrotron X-ray diffraction, Cryst. Growth Des. 13 (2013) 4031–4038, https://doi.org/10.1021/cg400835n.

[4] T.J. Headley, R.E. Loehman, Crystallization of a glass-ceramic by epitaxial growth, J. Am. Ceram. Soc. 67 (1984) 620–625, https://doi.org/10.1111/j.1151-2916.1984.tb19606.x.

[5] J. Deubener, R. Brückner, M. Sternitzke, Induction time analysis of nucleation and crystal growth in di- and metasilicate glasses, J. Non-Cryst. Solids 163 (1993) 1–12, https://doi.org/10.1016/0022-3093(93)90638-E.

[6] D. Holland, Y. Iqbal, P. James, B. Lee, Early stages of crystallisation of lithium disilicate glasses containing P_2O_5 – an NMR study, J. Non-Cryst. Solids 232–234 (1998) 140–146, https://doi.org/10.1016/S0022-3093(98)00381-0.

[7] I. Denry, J.A. Holloway, Ceramics for dental applications: a review, Materials 3 (2010) 351–368, https://doi.org/10.3390/ma3010351.

[8] F.C. Serbena, I. Mathias, C.E. Foerster, E.D. Zanotto, Crystallization toughening of a model glass-ceramic, Acta Mater. 86 (2015) 216–228, https://doi.org/10.1016/j.actamat.2014.12.007.

[9] P. Goharian, A. Nemati, M. Shabanian, A. Afshar, Properties, crystallization mechanism and microstructure of lithium disilicate glass–ceramic, J. Non-Cryst. Solids 356 (2010) 208–214, https://doi.org/10.1016/j.jnoncrysol.2009.11.015.

[10] S. Huang, B. Zhang, Z. Huang, W. Gao, P. Cao, Crystalline phase formation, microstructure and mechanical properties of a lithium disilicate glass–ceramic, J. Mater. Sci. 48 (2013) 251–257, https://doi.org/10.1007/s10853-012-6738-y.

[11] X. Huang, X. Zheng, G. Zhao, B. Zhong, X. Zhang, G. Wen, Microstructure and mechanical properties of zirconia-toughened lithium disilicate glass–ceramic composites, Mater. Chem. Phys. 143 (2014) 845–852, https://doi.org/10.1016/j.matchemphys.2013.10.023.

[12] P. Zhang, X. Li, J. Yang, S. Xu, Effect of heat treatment on the microstructure and properties of lithium disilicate glass-ceramics, J. Non-Cryst. Solids 402 (2014) 101–105, https://doi.org/10.1016/j.jnoncrysol.2014.05.023.

[13] W. Höland, M. Schweiger, M. Frank, V. Rheinberger, A comparison of the microstructure and properties of the IPS empress®2 and the IPS empress® glass-ceramics, J. Biomed. Mater. Res. 53 (n.d.) 297–303. doi: (10.1002/1097-4636(2000)53:4 < 297::AID-JBM3 > 3.0.CO;2-G).

[14] V. Imbeni, R.K. Nalla, C. Bosi, J.H. Kinney, R.O. Ritchie, In vitro fracture toughness of human dentin, J. Biomed. Mater. Res. A 66A (2003) 1–9, https://doi.org/10.1002/jbm.a.10548.

[15] R.K. Nalla, J.H. Kinney, R.O. Ritchie, Effect of orientation on the in vitro fracture toughness of dentin: the role of toughening mechanisms, Biomaterials. 24 (2003) 3955–3968, https://doi.org/10.1016/S0142-9612(03)00278-3.

[16] W. Höland, V. Rheinberger, M. Schweiger, Control of nucleation in glass ceramics, Philosophical Transactions of the Royal Society of London A 361 (2003) 575–589, https://doi.org/10.1098/rsta.2002.1152.

[17] X. Zheng, G. Wen, L. Song, X.X. Huang, Effects of P_2O_5 and heat treatment on crystallization and microstructure in lithium disilicate glass ceramics, Acta Mater. 56 (2008) 549–558, https://doi.org/10.1016/j.actamat.2007.10.024.

[18] S.C. von Clausbruch, M. Schweiger, W. Höland, V. Rheinberger, The effect of P_2O_5 on the crystallization and microstructure of glass-ceramics in the SiO_2–Li_2O–K_2O–ZnO–P_2O_5 system, J. Non-Cryst. Solids 263–264 (2000) 388–394, https://doi.org/10.1016/S0022-3093(99)00647-X.

[19] W. Höland, E. Apel, C. Van't Hoen, V. Rheinberger, Studies of crystal phase formations in high-strength lithium disilicate glass–ceramics, J. Non-Cryst. Solids 352 (2006) 4041–4050, https://doi.org/10.1016/j.jnoncrysol.2006.06.039.

[20] W. Lien, H.W. Roberts, J.A. Platt, K.S. Vandewalle, T.J. Hill, T.-M.G. Chu, Microstructural evolution and physical behavior of a lithium disilicate glass–-ceramic, Dent. Mater. 31 (2015) 928–940, https://doi.org/10.1016/j.dental.2015.05.003.

[21] Ivoclar Vivadent, Scientific Documentation: IPS e.max CAD-on, (2010).

[22] H.M. Rietveld, A profile refinement method for nuclear and magnetic structures, J. Appl. Crystallogr. 2 (1969) 65–71, https://doi.org/10.1107/S0021889869006558.

[23] B.H. Toby, R factors in Rietveld analysis: how good is good enough? Powder Diffract. 21 (2006) 67–70, https://doi.org/10.1154/1.2179804.

[24] J. Rodriguez-Carjaval, FullProf: A Program for Rietveld Refinement and Profile Matching Analysis of Complex Powder Diffraction Patterns, Laue-Langevin Institute, Grenoble, France.

[25] J. Rodríguez-Carvajal, Recent advances in magnetic structure determination by neutron powder diffraction, Phys. B Condens. Matter 192 (1993) 55–69, https://doi.org/10.1016/0921-4526(93)90108-I.

[26] A. Le Bail, Modelling the silica glass structure by the Rietveld method, J. Non-Cryst. Solids 183 (1995) 39–42, https://doi.org/10.1016/0022-3093(94)00664-4.

[27] L. Lutterotti, R. Ceccato, R. Dal Maschio, E. Pagani, Quantitative analysis of silicate glass in ceramic materials by the Rietveld method, Mater. Sci. Forum 278–281 (1998) 87, https://doi.org/10.4028/www.scientific.net/MSF.278-281.87.

[28] D.B. Peacor, High-temperature single-crystal study of the cristobalite inversion, Z. Krist. 138 (1973) 274–298, https://doi.org/10.1524/zkri.1973.138.jg.274.

[29] B. Hallstedt, Thermodynamic assessment of the silicon - oxygen system, Calphad. 16 (1992) 53–61, https://doi.org/10.1016/0364-5916(92)90038-Y.

[30] D.M. Hatch, S. Ghose, The α-β phase transition in cristobalite, SiO_2, Phys Chem Minerals. 17 (1991) 554–562, https://doi.org/10.1007/BF00202234.

[31] G. Wen, X. Zheng, L. Song, Effects of P_2O_5 and sintering temperature on microstructure and mechanical properties of lithium disilicate glass-ceramics, Acta Mater. 55 (2007) 3583–3591, https://doi.org/10.1016/j.actamat.2007.02.009.

[32] S.M. Johnson, R.H. Lamoreau, R.E. Loehman, Crystallization of a lithium silicate glass-ceramic under pressure, J. Am. Ceram. Soc. 78 (1995) 1115–1117, https://doi.org/10.1111/j.1151-2916.1995.tb08451.x.

[33] J.-C. Lee, Y.-C. Kim, J.-P. Ahn, H.-S. Kim, S.-H. Lee, B.-J. Lee, Deformation-induced nanocrystallization and its influence on work hardening in a bulk amorphous matrix composite, Acta Mater. 52 (2004) 1525–1533, https://doi.org/10.1016/j.actamat.2003.11.034.